Preclinical Characterization of the Tau PET Tracer [^{18}F]SNFT-1: Comparison of Tau PET Tracers

Ryuichi Harada[1,2], Pradith Lerdsirisuk[3], Yuki Shimizu[3], Yuka Yokoyama[3], Yiqing Du[1], Kaede Kudo[2], Michinori Ezura[4], Yoichi Ishikawa[3], Ren Iwata[3], Miho Shidahara[5], Aiko Ishiki[2,6], Akio Kikuchi[4], Yuya Hatano[7], Tomohiko Ishihara[7], Osamu Onodera[7], Yasushi Iwasaki[8], Mari Yoshida[8], Yasuyuki Taki[2], Hiroyuki Arai[2], Yukitsuka Kudo[2], Kazuhiko Yanai[3], Shozo Furumoto[3], and Nobuyuki Okamura[2,9]

[1]Department of Pharmacology, Tohoku University Graduate School of Medicine, Sendai, Japan; [2]Division of Brain Science, Department of Aging Research and Geriatric Medicine, Institute of Development, Aging, and Cancer, Tohoku University, Sendai, Japan; [3]Cyclotron and Radioisotope Center, Tohoku University, Sendai, Japan; [4]Department of Neurology, Tohoku University Graduate School of Medicine, Sendai, Japan; [5]Department of Quantum Science and Energy Engineering, Tohoku University, Sendai, Japan; [6]Division of Community Medicine, Tohoku Medical and Pharmaceutical University, Sendai, Japan; [7]Department of Neurology, Brain Research Institute, Niigata University, Niigata, Japan; [8]Department of Neuropathology, Institute for Medical Science of Aging, Aichi Medical University, Nagakute, Japan; and [9]Division of Pharmacology, Faculty of Medicine, Tohoku Medical and Pharmaceutical University, Sendai, Japan

Tau PET tracers are expected to be sufficiently sensitive to track the progression of age-related tau pathology in the medial temporal cortex. The tau PET tracer *N*-(4-[^{18}F]fluoro-5-methylpyridin-2-yl)-7-aminoimidazo[1,2-a]pyridine ([^{18}F]SNFT-1) has been successfully developed by optimizing imidazo[1,2-a]pyridine derivatives. We characterized the binding properties of [^{18}F]SNFT-1 using a head-to-head comparison with other reported ^{18}F-labeled tau tracers. **Methods:** The binding affinity of SNFT-1 to tau, amyloid, and monoamine oxidase A and B was compared with that of the second-generation tau tracers MK-6240, PM-PBB3, PI-2620, RO6958948, JNJ-64326067, and flortaucipir. In vitro binding properties of ^{18}F-labeled tau tracers were evaluated through the autoradiography of frozen human brain tissues from patients with diverse neurodegenerative disease spectra. Pharmacokinetics, metabolism, and radiation dosimetry were assessed in normal mice after intravenous administration of [^{18}F]SNFT-1. **Results:** In vitro binding assays demonstrated that [^{18}F]SNFT-1 possesses high selectivity and high affinity for tau aggregates in Alzheimer disease (AD) brains. Autoradiographic analysis of tau deposits in medial temporal brain sections from patients with AD showed a higher signal-to-background ratio for [^{18}F]SNFT-1 than for the other tau PET tracers and no significant binding with non-AD tau, α-synuclein, transactiviation response DNA-binding protein-43, and transmembrane protein 106B aggregates in human brain sections. Furthermore, [^{18}F]SNFT-1 did not bind significantly to various receptors, ion channels, or transporters. [^{18}F]SNFT-1 showed a high initial brain uptake and rapid washout from the brains of normal mice without radiolabeled metabolites. **Conclusion:** These preclinical data suggest that [^{18}F]SNFT-1 is a promising and selective tau radiotracer candidate that allows the quantitative monitoring of age-related accumulation of tau aggregates in the human brain.

Key Words: tau; radiotracers; PET; misfolded proteins, comparison

J Nucl Med 2023; 64:1495–1501
DOI: 10.2967/jnumed.123.265593

Received Feb. 24, 2023; revision accepted May 3, 2023.
For correspondence or reprints, contact Ryuichi Harada (ryuichi.harada.c8@tohoku.ac.jp).
Published online Jun. 15, 2023.

Misfolded tau aggregates are the neuropathologic hallmarks of Alzheimer disease (AD). In the AD continuum, the progression of tau pathology follows a stereotyped spatiotemporal pattern that begins in the transentorhinal cortex and spreads to the entorhinal and hippocampal cortices, lateral temporal lobes, and association and primary sensory cortices (*1*). Pathologic tau aggregates are associated with neuronal loss and cognitive decline in AD (*2*). PET imaging with specific tau tracers provides spatiotemporal information on the progression of pathologic tau burden in the living brain and facilitates the precise assessment of disease severity, patient enrollment, and prediction of therapeutic efficacy in disease-modifying therapeutic trials (*3*).

Much effort over the past 10 y has been focused on generating radiotracers to visualize tau aggregates in vivo. We previously developed ^{18}F-labeled 2-arylquinoline derivatives to image pathologic tau aggregates in humans (*3*). One of these derivatives, [^{18}F]THK-5351, showed elevated tracer retention at sites susceptible to pathologic tau burden in AD. However, the off-target binding to monoamine oxidase B (MAO-B) limits the clinical utility of [^{18}F]THK-5351 as a tau biomarker (*4,5*). Off-target binding issues have been noted in other first-generation tau tracers that show high uptake in the basal ganglia and choroid plexus even in normal control brains. To overcome this issue, second-generation tau PET tracers such as [^{18}F]RO6958948 ([^{18}F]RO948), [^{18}F]PI-2620, [^{18}F]MK-6240, [^{18}F]JNJ-64326067 ([^{18}F]JNJ-067), and [^{18}F]PM-PBB3 have been developed to reduce off-target binding to monoamine oxidase (*6*). Clinical studies of these radiotracers have demonstrated less off-target binding to MAO-B, although several tracers still showed significant accumulation in the choroid plexus. Additionally, the existing tau tracers are not sufficiently sensitive to track the progression of early tau lesions. Large antemortem PET-autopsy validation studies have revealed that [^{18}F]flortaucipir PET detected advanced tau pathology (Braak V–VI) but was not sensitive in detecting early tau burden (Braak I–IV) (*7,8*). To develop a novel tau tracer with high sensitivity and specificity to tau pathology in AD, we performed the compound optimization of imidazo[1,2-a]pyridine derivatives and developed *N*-(4-[^{18}F]fluoro-5-methylpyridin-2-yl)-7-aminoimidazo[1,2-a]pyridine ([^{18}F]SNFT-1) as

an optimized tau PET tracer (Fig.1). We directly compared the binding profile of [^{18}F]SNFT-1 with that of other reported tau PET tracers using human brain tissues from patients with a diverse disease spectrum.

MATERIALS AND METHODS

Radiochemistry

Reference standards and their precursors were custom-synthesized or synthesized in-house on the basis of patents or the literature. LogP values were estimated by reversed-phase high-performance liquid chromatography as described in the supplemental methods (supplemental materials are available at http://jnm.snmjournals.org) (*9*). Radiolabeled compounds were obtained through a microscale ^{18}F-substitution reaction, as previously described (*10*). Details of SNFT-1 and [^{18}F]SNFT-1 syntheses have been described elsewhere. Briefly, reactive [^{18}F]fluoride was prepared using an Oasis MAX (Waters) and a methanolic solution of the Kryptofix (Merck) 222–$KHCO_3$ complex. After drying, each precursor was dissolved in dimethyl sulfoxide (3 mg/mL). The vial was heated at 110°C–150°C in a block heater. After radiofluorination, acid deprotection was performed to remove the protecting groups. [^{18}F]RO948 and [^{18}F]PI-2620 were prepared by reducing with iron powder to remove the nitro precursors. The quenched solution was subjected to semipreparative high-performance liquid chromatography (InertSustain C18 column, 7.6 × 150 mm and 5 μm; GL Sciences, Inc.). The products were extracted from the collected fraction with ethanol using a Sep-Pak tC18 Plus Light (Waters) cartridge and diluted with appropriate buffers for biologic assays. All products were produced in more than 95% radiochemical purity, which was determined using analytic high-performance liquid chromatography (InertSustain C18 column, 4.6 × 150 mm and 5 μm; GL Sciences, Inc.). The molar activities are presented in Supplemental Table 1.

In Vitro Binding Studies

[^{3}H]THK-5351 was custom-synthesized by Sekisui Medical, Inc. (molar activity, 2.96 TBq/mmol; radiochemical purity, 98.9%). [^{3}H]Pittsburgh compound B (PiB) was obtained from American Radiolabeled Chemicals, Inc. (molar activity, 2.96 TBq/mmol; radiochemical purity, 99%). Competitive binding assays were performed as described previously (*11*). [^{18}F]florbetaben and [^{3}H]PiB were used as radioligands for the amyloid aggregates; [^{18}F]MK-6240, [^{18}F]SNFT-1, and [^{18}F]PM-PBB3 were used for 3-repeat/4-repeat (3R/4R) tau aggregates; [^{18}F]fluoroethyl harmol was used for recombinant MAO-A (M7316; Sigma-Aldrich); and [^{3}H]THK-5351 was used for recombinant MAO-B (M7441; Sigma-Aldrich). Correlation analysis of tracer binding in an AD patient was performed as described previously (*5,11*). The Sidak multiple-comparison test was used to investigate statistical significance.

In Vitro Autoradiography, Histochemical Staining, and Immunoblotting

The Ethics Committee of Tohoku University Graduate School of Medicine approved this study, and all subjects gave written informed consent. The demographic data of the postmortem brain samples are shown in Supplemental Table 2. In vitro autoradiography of ^{18}F-labeled compounds was performed using unfixed frozen brain sections as previously described (*11,12*). Quantitative tracer binding was evaluated as the ratio of the region of interest to a region of white matter. Detailed histochemical staining and immunoblotting are described in the supplemental methods.

Receptor Binding Assays

Receptor binding screening assays were performed by Sekisui Medical, Inc., to confirm the binding selectivity of [^{18}F]SNFT-1 to tau. Binding inhibition (%) was determined using competitive radioligand assays against 60 common neurotransmitter receptors, ion channels, and transporters as described previously (*11,13*).

Biodistribution, Small-Animal PET, and Metabolism Studies on Mice

All animal experimental protocols were approved by the Laboratory Animal Care Committee of the Tohoku University. Biodistribution and metabolism were investigated after intravenous injection of [^{18}F]SNFT-1 into male ICR mice, as described previously (*13,14*). Details on the metabolite analysis are described in the supplemental methods. A small-animal PET study was performed as previously described (*15*). Estimations of radiation and mass doses for humans were based on biodistribution data as previously described (*16*).

Animal Toxicity Studies

Acute toxicity studies were performed on Sprague–Dawley rats and ICR mice. A single intravenous dose of SNFT-1 was administered by LSI Medience as previously described (*11,13*).

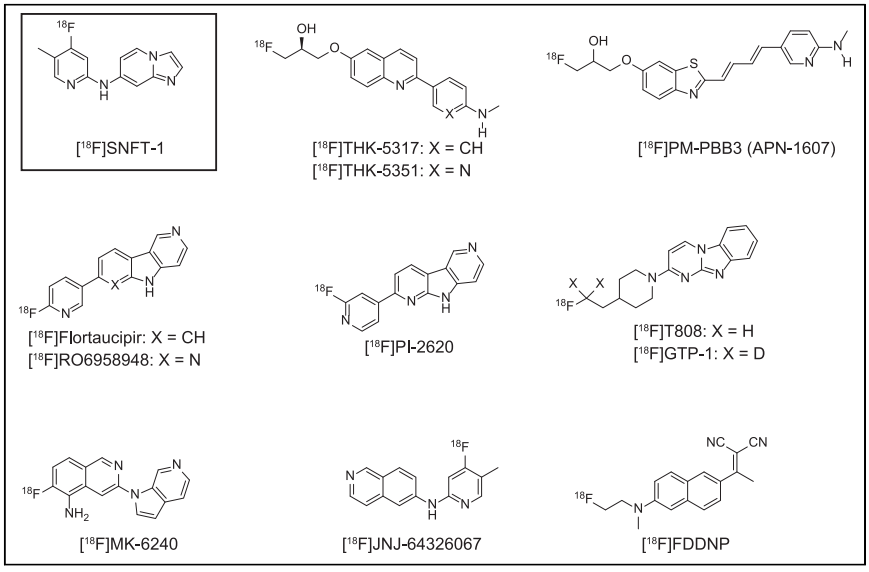

FIGURE 1. Chemical structures of clinically evaluated ^{18}F-labeled tau PET tracers and [^{18}F]SNFT-1.

RESULTS

In Vitro Binding Studies

The results of the in vitro saturation binding assay of [^{18}F]SNFT-1 are shown in Figure 2A. [^{18}F]SNFT-1 bound with high affinity to 2 binding sites on tau-rich AD brain homogenates (high dissociation constant, 0.6 nmol/L; high maximum number of binding sites, 303 pmol/g tissue; low dissociation constant, 57.6 nmol/L; low maximum number of binding sites, 3,140 pmol/g tissue). The regional binding ratios of [^{18}F]SNFT-1 in AD brain samples correlated strongly with those of [^{18}F]MK-6240 (Spearman $r = 0.97$, $P < 0.0001$) (Fig. 2B) and did not correlate with those of [^{3}H]PiB (Spearman $r = 0.28$, $P = 0.31$) (Supplemental Fig. 1). The regional binding ratio of [^{18}F]SMBT-1 was higher than that of [^{18}F]MK-6240 in several regions of the brain (Fig. 2C). In vitro competitive binding assays were performed to

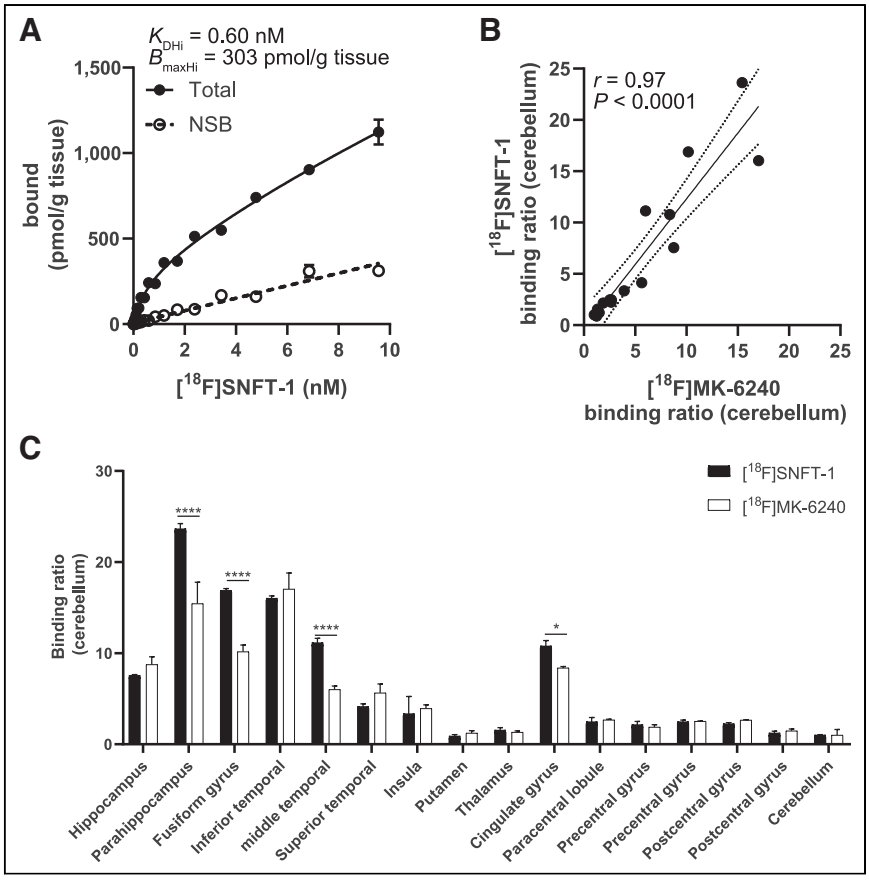

FIGURE 2. (A) Saturation binding assay of [^{18}F]SNFT-1 against inferior temporal brain homogenate from patient with AD. (B) Correlation of binding ratio between [^{18}F]SNFT-1 and [^{18}F]MK-6240 against AD brain homogenate (Braak VI). (C) Regional binding ratio of [^{18}F]SNFT-1 and [^{18}F]MK-6240 in AD case. B_{maxHi} = high maximum number of binding sites; K_{DHi} = high dissociation constant; NSB = nonspecific binding. *$P < 0.05$. ****$P < 0.0001$.

compare the binding affinity and selectivity of SNFT-1 with those of other reported tau tracers for 3R/4R tau aggregates (Table 1). SNFT-1 showed high affinity for 3R/4R tau aggregates (half-maximal inhibitory concentration [IC_{50}], 0.84 nM) but low binding affinity (IC_{50} > 1,000 nM) for MAO enzymes and amyloid aggregates. THK-5351 and FDDNP showed high binding affinity for MAO-B (THK-5351 IC_{50}, 5.2 nM; FDDNP IC_{50}, 6.5 nM), and flortaucipir showed high binding affinity for MAO-A (IC_{50}, 8.8 nM). The second-generation tau tracers showed high selectivity for 3R/4R tau aggregates, but PM-PBB3 showed moderate binding affinity for amyloid aggregates (IC_{50}, 12.8 nM). To further characterize the binding sites of tau PET tracers, in vitro competitive binding to 3R/4R tau aggregates was examined using [^{18}F]MK-6240, [^{18}F]SNFT-1, and [^{18}F]PM-PBB3 as radioligands (Supplemental Fig. 1). [^{18}F]SNFT-1 binding competed with binding of MK-6240 and flortaucipir at low nanomolar concentrations, and [^{18}F]MK-6240 binding competed with binding of SNFT-1 and flortaucipir at low nanomolar concentrations. [^{18}F]PM-PBB3 binding did not compete with binding of MK-6240, flortaucipir, and SNFT-1 but partially competed with binding of PiB (~80%; IC_{50}, 88.9 nM), and PM-PBB3 competed with the binding site of [^{3}H]PiB (IC_{50}, 9.9 nM). The IC_{50} values of tau PET tracers determined using [^{18}F]SNFT-1 correlated well with those determined using [^{18}F]MK-6240.

TABLE 1
LogP and Binding Affinities

Compounds	HPLC LogP	Binding affinities			
		Tau aggregates*	Amyloid aggregates	MAO-A	MAO-B
SNFT-1	1.34	0.84	>1,000	>1,000	>1,000
MK-6240	2.11	0.64	>1,000	>1,000	>1,000
PM-PBB3	2.00	28.4 (14.4 nM†)	12.8	>1,000	>1,000
PI-2620	1.34	1.32	>1,000	>1,000	>1,000
JNJ-067	2.38	1.07	>1,000	568	58.9
RO948	1.19	1.63	>1,000	>1,000	249
THK-5351	1.28	19.0	771	>1,000	5.2
Flortaucipir	1.65	0.28	>1,000	8.8	55.3
T808	1.96	2.16	>1,000	>1,000	>1,000
FDDNP	3.68	693	902	>1,000	6.5

*[^{18}F]MK-6240 (2.3 nM) was used as radioligand.
†[^{18}F]PM-PBB3 (2.5 nM) was used as radioligand.
HPLC = high-performance liquid chromatography.
Binding affinities are IC_{50} (nM).

Receptor-binding screening assays also confirmed that no remarkable interaction was detected between SNFT-1 and various receptors, ion channels, or transporters (Supplemental Table 3).

In Vitro Autoradiography of Postmortem Human Brain Sections

To further characterize the binding of [^{18}F]SNFT-1 at early stages of tau pathology in the human brain, in vitro autoradiography was performed using medial temporal brain sections from individuals with low (II) and high (VI) Braak stages. [^{18}F]SNFT-1 clearly visualized tau deposits in the entorhinal cortex brain sections with presentations of Braak stage II. Strong [^{18}F]SNFT-1 signals were detected in the medial temporal cortex of Braak stage VI brain samples. The spatial pattern of [^{18}F]SNFT-1 binding was consistent with that observed using tau immunohistochemistry (Fig. 3). Similar to [^{18}F]SNFT-1, other tau tracers ([^{18}F]MK-6240, [^{18}F]PM-PBB3, [^{18}F]PI-2620, [^{18}F]RO-948, [^{18}F]JNJ-067, and [^{18}F]flortaucipir) specifically bound to the area of tau deposition (Fig. 3; Supplemental Fig. 2). [^{18}F]PM-PBB3 showed greater binding in the uncus of the hippocampus than did the other tau PET tracers (Supplemental Fig. 2). [^{18}F]SNFT-1 and [^{18}F]MK-6240 showed no remarkable binding in the choroid plexus, unlike the prominent signal of [^{18}F]PM-PBB3 in the choroid plexus (Fig. 3).

In contrast to the results from AD brain sections, no significant binding of [^{18}F]SNFT-1 was detected in progressive supranuclear palsy brain sections, except in patient 6 (progressive supranuclear palsy). Specific [^{18}F]SNFT-1 signals in patient 6 corresponded to tau immunohistochemistry (Fig. 4). Immunoblot analysis of sarkosyl-insoluble tau in patient 6 showed 3 bands corresponding to hyperphosphorylated full-length tau (60, 64, and 68 kDa) detected using T46 (anti-tau C terminus) and 2 major bands (60 and 64 kDa) detected using RD3 (anti-three-repeat tau) (Fig. 4); these results were consistent with those of AD, suggesting concomitant binding in AD pathology. [^{18}F]SNFT-1 showed no remarkable binding to α-synuclein in the brain sections with presentation of multiple-system atrophy or to transactivation response DNA-binding protein (TDP-43) or transmembrane protein 106B (TMEM106B) in the brain sections with presentation of frontotemporal lobar degeneration (FTLD), although TMEM106B aggregates were stained with a fluorescent cross β-sheet ligand, BF-188 (Fig. 5).

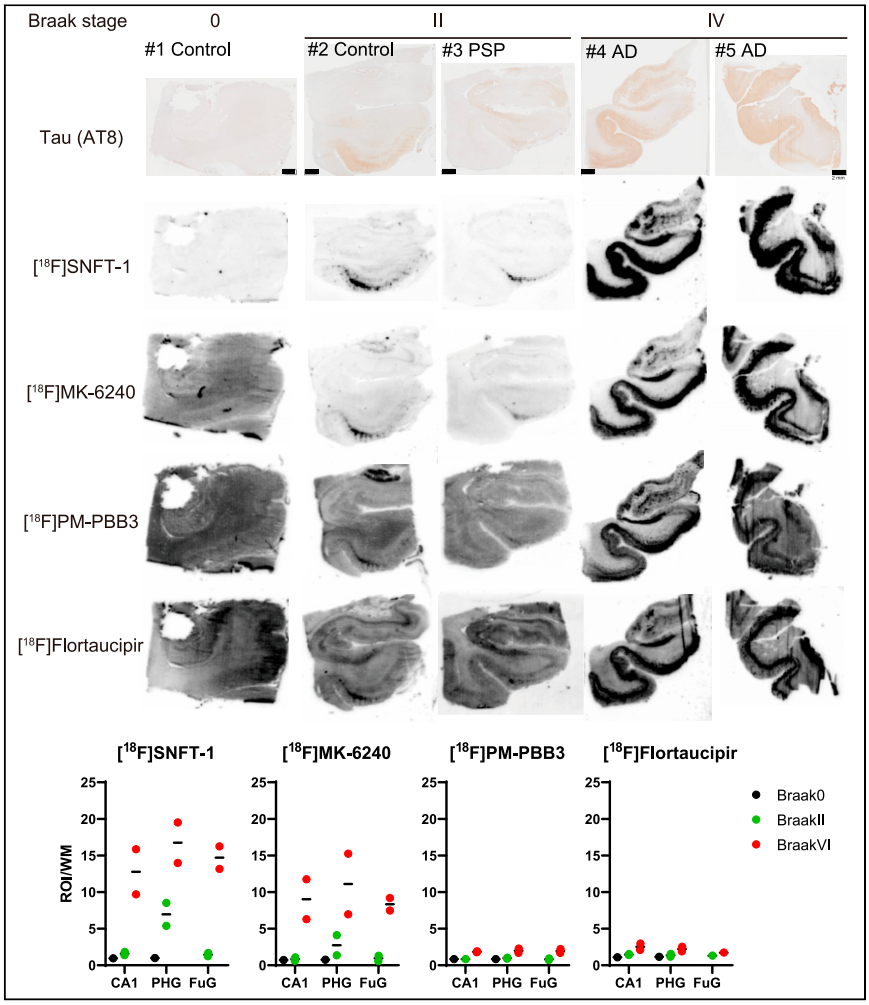

FIGURE 3. Tau immunohistochemistry and in vitro autoradiograms of [^{18}F]SNFT-1, [^{18}F]]MK-6240, [^{18}F]PM-PBB3, and [^{18}F]flortaucipir in medial temporal sections from cases presenting different Braak stages (AD spectrum). AT8 = anti-phosphorylated tau antibody; CA1 is the region in the hippocampus circuit; FuG = fusiform gyrus; PHG = parahippocampal gyrus; PSP = progressive supranuclear palsy; ROI = region of interest; WM = white matter.

Biodistribution and Metabolism of [^{18}F]SNFT-1 in Mice

[^{18}F]SNFT-1 entered the brain immediately after being injected intravenously and was rapidly washed out in mice without significant defluorination (Fig. 6; Supplemental Table 4). Estimation of [^{18}F]SNFT-1 radiation exposure was based on the biodistribution data of mice (Supplemental Table 5). The resultant whole-body effective dose equivalents were 14.1 μSv/MBq (male) and 17.5 μSv/MBq (female). [^{18}F]SNFT-1 was rapidly metabolized in mice. At 10 min after injection, only 8% of the parent [^{18}F]SNFT-1 remained in the plasma, whereas 2 polar radiolabeled metabolites were observed. In contrast, all radioactivity in the brain was derived from the parent during the 10-min period after intravenous administration (Supplemental Fig. 3).

Animal Toxicity Studies

A single intravenous administration of SNFT-1 at 1 mg/kg, which is 100,000-fold the intended clinical dose in humans, caused no systemic toxicity in rats or mice.

DISCUSSION

We previously developed ^{18}F-labeled 2-arylquinoline derivatives for imaging pathologic tau aggregates (*3*). [^{18}F]THK-5351 PET studies showed prominent tracer retention in both AD and non-AD brains and nonnegligible tracer retention in the basal ganglia and thalamus (*17*). Further validation studies have shown that MAO-B is an off-target binding site for [^{18}F]THK-5351, which limits the clinical utility of [^{18}F]THK-5351 as a tau biomarker (*4,5*). However, [^{18}F]THK-5351 PET studies have

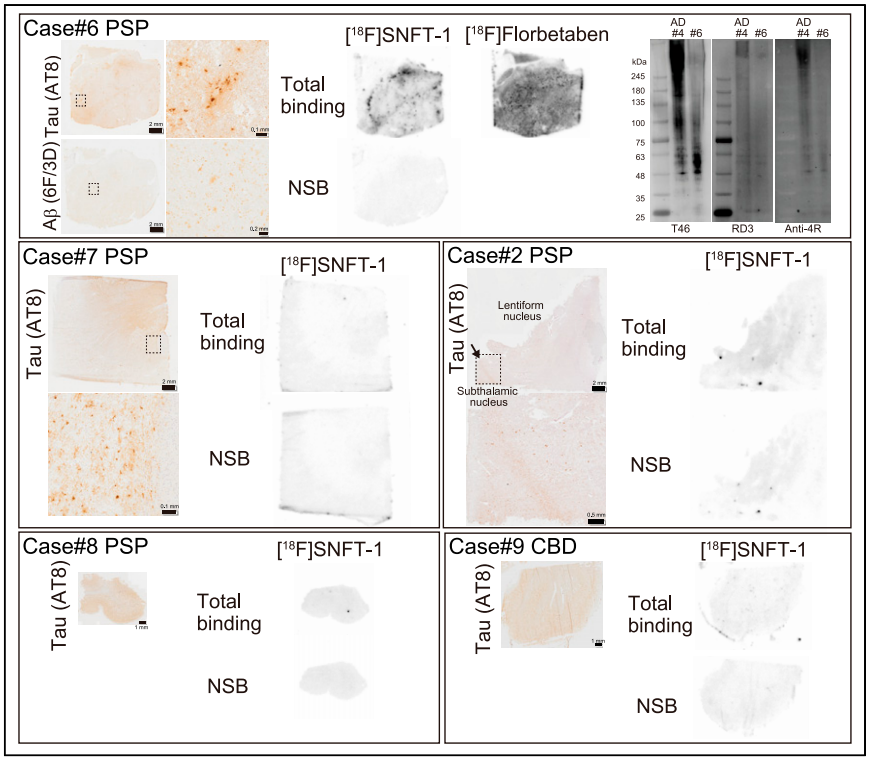

FIGURE 4. In vitro autoradiograms of [^{18}F]SNFT-1 and tau immunohistochemistry against sections presenting non-AD tauopathies. AT8 = anti-phosphorylated tau antibody; NSB = nonspecific binding; PSP = progressive supranuclear palsy.

suggested that MAO-B is a promising target for the PET imaging of reactive astrogliosis. Therefore, we developed [^{18}F]SMBT-1 through compound optimization of [^{18}F]THK-5351 to reduce its binding affinity for tau aggregates (*11*). We additionally performed lead optimization of THK-5351 derivatives to generate a selective tau PET tracer (*18*). The optimized tracer, [^{18}F]SNFT-1, showed high binding affinity and selectivity against pathologic tau aggregates in AD as evidenced in the in vitro binding assay (dissociation constant, 0.6 nM) (Fig. 2). A head-to-head comparison of tau PET tracer performance in the autoradiography of AD brains demonstrated similar binding patterns among the tau PET tracers. This finding was similar to that of a previous comparative autoradiography study of [^{3}H]RO948, [^{3}H]PI-2620, [^{3}H]MK-6240, and [^{3}H]JNJ-067 (*19*). However, the signal-to-background ratios differed between the tracers (Fig. 3; Supplemental Fig. 2). The signal-to-background ratio of [^{18}F]SNFT-1 is superior to that of second-generation tau tracers. We performed comparative autoradiography of tau PET tracers under the same experimental conditions without using alcohols for the fixation and differentiation processes because alcohols reduce nonspecific radiotracer binding and enhance signal-to-background ratio (*20,21*). Therefore, our results are expected to accurately reflect the binding properties of PET tracers under physiologic conditions. These findings support the superiority of [^{18}F]SNFT-1 in detecting early (Braak I–IV) tau pathology in the AD continuum.

Recent innovations in cryoelectron microscopy have revealed the atomic structure of the tau PET ligand–tau aggregate complex, identifying 2 major binding sites of PM-PBB3 in the β-helix of paired helical filaments and straight filaments and a third major site in the C-shaped cavity of straight filaments (*22*). The competitive binding assay indicated that [^{18}F]SNFT-1 shares the binding sites with MK-6240 but not with PM-PBB3 (Supplemental Fig. 1). The binding sites of PM-PBB3 were unique among the tau PET tracers; nevertheless, [^{3}H]PiB partially competed with the binding sites of [^{18}F]PM-PBB3 (IC_{50}, 88.9 nM). A study that originally used BTA-1 (IC_{50}, 379.1 nM) reported similar results (*23*). Additionally, recent autoradiographic studies have demonstrated off-target binding of PM-PBB3 to amyloid-β as evidenced by displacement with NAV-4694 (*24,25*).

[^{18}F]flortaucipir PET studies have been reported to recapitulate Braak stages that follow stereotypic spatiotemporal patterns (*26,27*). Autoradiography studies have shown that [^{18}F]flortaucipir binding correlates well with tau immunohistochemistry across different Braak stages (*28*). However, autopsy validation studies demonstrated that [^{18}F]flortaucipir PET could detect advanced tau pathology (Braak V–VI) but had low sensitivity for detecting early tau burden (Braak I–IV) (*7,8*). Here, [^{18}F]flortaucipir was less sensitive in detecting Braak stage II tau lesions than was [^{18}F]SNFT-1, possibly because of a higher background signal. The presence of the selective MAO-A inhibitor clorgyline enhanced the signal-to-background ratio in

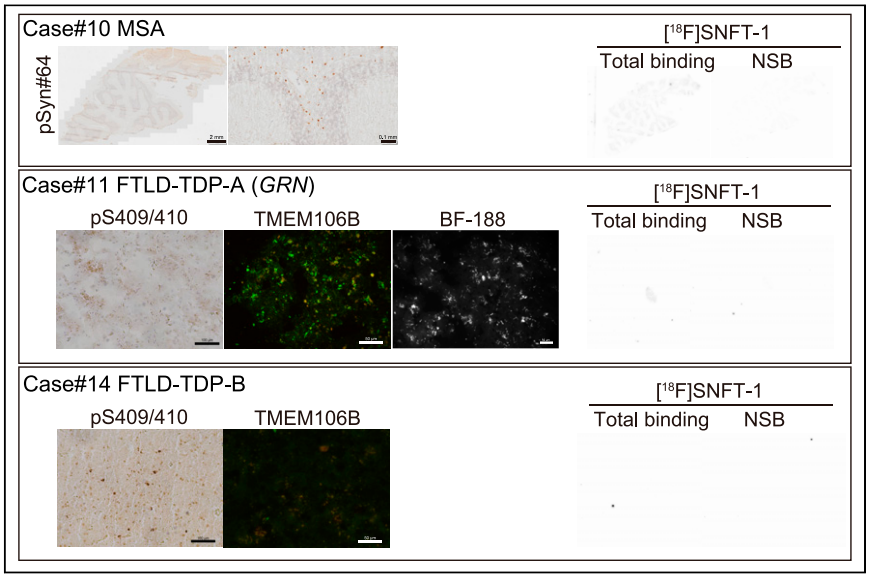

FIGURE 5. In vitro autoradiograms of [^{18}F]SNFT-1, immunohistochemical markers (α-synuclein, TDP-43, and TMEM106B), and BF-188 staining against sections presenting multiple-system atrophy and TDP-43 proteinopathies. *GRN* = progranulin gene; MSA = multiple-system atrophy; NSB = nonspecific binding.

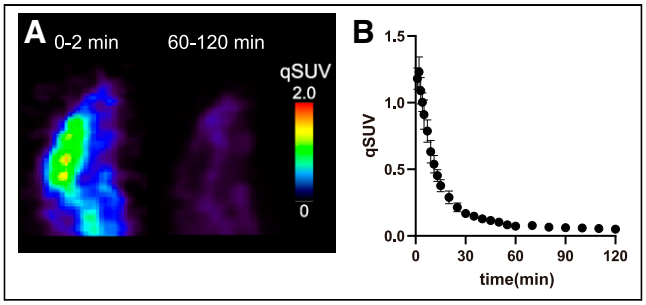

FIGURE 6. (A) Representative PET images of [^{18}F]SNFT-1 at 0–2 min and 60–120 min after its injection in normal mice. (B) Brain time–activity curves after intravenous administration of [^{18}F]SNFT-1 in normal mice (n = 4). qSUV = quasi-SUV.

samples of early Braak stages (Supplemental Fig. 4), suggesting that off-target binding of [^{18}F]flortaucipir to MAO-A interferes with the detection of Braak stage II tau pathology. Nevertheless, a recent study reported that binding of [^{18}F]flortaucipir to MAO-A does not affect the PET signal in cortical target areas (*29*). Recent clinical studies on [^{18}F]MK-6240 have demonstrated early detection of tau aggregates in the entorhinal cortex (*30,31*). The signal-to-background ratio of [^{18}F]SNFT-1 was equivalent to that of [^{18}F]MK-6240, indicating the potential usefulness of [^{18}F]SNFT-1. Furthermore, [^{18}F]SNFT-1 exhibited little binding to the choroid plexus in vitro. [^{18}F]PM-PBB3 showed high binding to the choroid plexus, which is consistent with that observed in vivo (*23*). Second-generation tau PET tracers showed less off-target binding to the basal ganglia but higher binding to the skull or meninges in some individuals. Prediction of the in vivo off-target binding of new PET tracers in humans based only on the results of preclinical studies is challenging. Numerous factors, such as metabolic, target, and methodologic issues, often hinder the successful translation of the new tracers to clinical PET imaging. Future investigations are needed to associate the in vitro and in vivo characteristics of [^{18}F]SNFT-1 binding and metabolism.

[^{18}F]flortaucipir showed elevated tracer retention in regions that are expected to harbor tau pathology in non-AD tauopathies such as progressive supranuclear palsy and chronic traumatic encephalopathy (*32,33*). However, in vitro autoradiography studies have demonstrated no significant specific binding in brain sections in non-AD cases (*32,34*). Although most second-generation tau tracers do not bind to non-AD tau aggregates, [^{18}F]PI-2620 and [^{18}F]PM-PBB3 have been reported to detect non-AD tau aggregates (*23,35*). [^{18}F]FDDNP, which was the first reported PET tracer for imaging amyloid and tau aggregates in AD brains (*36*), showed high binding affinity for MAO-B (IC_{50}, 6.5 nM). [^{18}F]FDDNP PET studies have demonstrated elevated tracer retention in the medial temporal lobe and neocortex in AD and in sites susceptible to tau burden in progressive supranuclear palsy and chronic traumatic encephalopathy (*36–38*), implying the possibility of [^{18}F]FDDNP binding to MAO-B. Here, [^{18}F]SNFT-1 did not show specific binding in non-AD cases when concomitant AD pathology was absent. Recently, in vitro head-to-head comparisons of ^{3}H-labeled tau PET ligands, including [^{3}H]MK-6240, [^{3}H]JNJ-067, [^{3}H]GTP-1, [^{3}H]CBD-2115, and [^{3}H]PM-PBB3, were reported in sections of postmortem amyotrophic lateral sclerosis brain containing phosphorylated TDP-43 (*24*). No evidence of binding of phosphorylated TDP-43 aggregates to any of the tau PET ligands exists, nor did [^{18}F]SNFT-1 bind to phosphorylated TDP-43 aggregates in FTLD-TDP (Fig. 5). Recent cryoelectron microscopy analyses identified TMEM106B as a novel protein filament in postmortem brain tissues from various neurodegenerative conditions and normal aging (*39–41*). A recent neuropathologic investigation reported that all cases of frontotemporal dementia caused by mutations in the progranulin gene showed high levels of TMEM106B aggregates (*42*); they are present in a wide range of brain cell types, including the choroid plexus epithelium, and correlate strongly with age, suggesting that they are potential off-target substrates for tau PET tracers. The study reported a lack of staining for any of the special histochemical stains such as Congo red (*42*). However, a high density of thioflavin-S–positive astrocytosis was previously observed in the superficial frontal cortex of FTLD-TDP-A when stained with modified thioflavin-S (*43*); they seemed to be TMEM106B aggregates because immunoreactivity was highest in astrocytes (*42*). Here, a fluorescent β-sheet binding ligand, BF-188, stained TMEM106B aggregates in FTLD-TDP-A (progranulin gene) (Fig. 5), whereas [^{18}F]SNFT-1 showed no evidence of binding with TMEM106B aggregates. Thus, [^{18}F]SNFT-1 appears to be a tau racer with high selectivity for paired-helical-filament tau.

CONCLUSION

[^{18}F]SNFT-1 is a promising selective PET tracer candidate for imaging tau aggregates in the AD spectrum. Future clinical studies are needed to ascertain the utility of this tracer in vivo.

DISCLOSURE

This study was supported by the Clino Ltd. Grant-in-Aid for Young Scientists (18K15538 and 18K15357), Grant-in-Aid for Scientific Research (B) (18H02771), Grant-in-Aid for Scientific Research on Innovative Areas (Brain Protein Aging and Dementia Control) (26117003), and Grant-in-Aid for Fostering Joint International Research (B) (19KK0212) from MEXT; the Strategic Research Program for Brain Science (JP20dm0107157 and JP21ab0123456) from the Japan Agency for Medical Research and Development; and the Grant-in-Aid for Joint Research by Young Researchers from Shimadzu Science Foundation. Yukitsuka Kudo and Nobuyuki Okamura own stock in Clino Ltd. Ryuichi Harada, Pradith Lerdsirisuk, Yukitsuka Kudo, Shozo Furumoto, and Nobuyuki Okamura have pending patents for the technology described in this paper. No other potential conflict of interest relevant to this article was reported.

ACKNOWLEDGMENTS

We thank the staff at the Cyclotron and Radioisotope Center of Tohoku University for their help with the HM-12 cyclotron operation. We acknowledge the support of the Biomedical Research Core of the Tohoku University Graduate School of Medicine. We thank Prof. Tetsuyuki Kitamoto for neuropathologic examinations.

KEY POINTS

QUESTION: What are the preclinical properties, such as specific binding and off-target binding, of a newly generated tau PET tracer, [^{18}F]SNFT-1, compared with clinically applied second-generation tau PET tracers?

PERTINENT FINDINGS: [^{18}F]SNFT-1 possesses preferable pharmacokinetic profiles and high affinity and high selectivity for AD tau aggregates, with little nonspecific binding and off-target binding compared with clinically applied second-generation tau PET tracers.

IMPLICATIONS FOR PATIENT CARE: Our results indicate the potential use of [^{18}F]SNFT-1 for sensitive and selective detection of tau aggregates in humans.

REFERENCES

1. Braak H, Alafuzoff I, Arzberger T, Kretzschmar H, Del Tredici K. Staging of Alzheimer disease-associated neurofibrillary pathology using paraffin sections and immunocytochemistry. *Acta Neuropathol (Berl).* 2006;112:389–404.
2. Guillozet AL, Weintraub S, Mash DC, Mesulam MM. Neurofibrillary tangles, amyloid, and memory in aging and mild cognitive impairment. *Arch Neurol.* 2003; 60:729–736.
3. Okamura N, Harada R, Ishiki A, Kikuchi A, Nakamura T, Kudo Y. The development and validation of tau PET tracers: current status and future directions. *Clin Transl Imaging.* 2018;6:305–316.
4. Ng KP, Pascoal TA, Mathotaarachchi S, et al. Monoamine oxidase B inhibitor, selegiline, reduces ^{18}F-THK5351 uptake in the human brain. *Alzheimers Res Ther.* 2017;9:25.
5. Harada R, Ishiki A, Kai H, et al. Correlations of ^{18}F-THK5351 PET with postmortem burden of tau and astrogliosis in Alzheimer disease. *J Nucl Med.* 2018;59:671–674.
6. Leuzy A, Chiotis K, Lemoine L, et al. Tau PET imaging in neurodegenerative tauopathies: still a challenge. *Mol Psychiatry.* 2019;24:1112–1134.
7. Fleisher AS, Pontecorvo MJ, Devous MD Sr, et al. Positron emission tomography imaging with [^{18}F]flortaucipir and postmortem assessment of Alzheimer disease neuropathologic changes. *JAMA Neurol.* 2020;77:829–839.
8. Lowe VJ, Lundt ES, Albertson SM, et al. Tau-positron emission tomography correlates with neuropathology findings. *Alzheimers Dement.* 2020;16:561–571.
9. Harada R, Okamura N, Furumoto S, et al. Use of a benzimidazole derivative BF-188 in fluorescence multispectral imaging for selective visualization of tau protein fibrils in the Alzheimer's disease brain. *Mol Imaging Biol.* 2014;16:19–27.
10. Iwata R, Pascali C, Terasaki K, Ishikawa Y, Furumoto S, Yanai K. Minimization of the amount of Kryptofix 222 - $KHCO_3$ for applications to microscale ^{18}F-radiolabeling. *Appl Radiat Isot.* 2017;125:113–118.
11. Harada R, Hayakawa Y, Ezura M, et al. ^{18}F-SMBT-1: a selective and reversible PET tracer for monoamine oxidase-B imaging. *J Nucl Med.* 2021;62:253–258.
12. Ishiki A, Harada R, Kai H, et al. Neuroimaging-pathological correlations of [^{18}F]THK5351 PET in progressive supranuclear palsy. *Acta Neuropathol Commun.* 2018;6:53.
13. Okamura N, Furumoto S, Harada R, et al. Novel ^{18}F-labeled arylquinoline derivatives for noninvasive imaging of tau pathology in Alzheimer disease. *J Nucl Med.* 2013;54:1420–1427.
14. Harada R, Shimizu Y, Du Y, et al. The role of chirality of [^{18}F]SMBT-1 in imaging of monoamine oxidase-B. *ACS Chem Neurosci.* 2022;13:322–329.
15. Tago T, Furumoto S, Okamura N, et al. Preclinical evaluation of [^{18}F]THK-5105 enantiomers: effects of chirality on its effectiveness as a tau imaging radiotracer. *Mol Imaging Biol.* 2016;18:258–266.
16. Shidahara M, Tashiro M, Okamura N, et al. Evaluation of the biodistribution and radiation dosimetry of the ^{18}F-labelled amyloid imaging probe [^{18}F]FACT in humans. *EJNMMI Res.* 2013;3:32.
17. Harada R, Okamura N, Furumoto S, et al. ^{18}F-THK5351: a novel PET radiotracer for imaging neurofibrillary pathology in Alzheimer disease. *J Nucl Med.* 2016;57:208–214.
18. Lerdsirisuk P, Harada R, Hayakawa Y, et al. Synthesis and evaluation of 2-pyrrolopyridinylquinoline derivatives as selective tau PET tracers for the diagnosis of Alzheimer's disease. *Nucl Med Biol.* 2021;93:11–18.
19. Yap SY, Frias B, Wren MC, et al. Discriminatory ability of next-generation tau PET tracers for Alzheimer's disease. *Brain.* 2021;144:2284–2290.
20. Marquié M, Normandin MD, Vanderburg CR, et al. Validating novel tau positron emission tomography tracer [F-18]-AV-1451 (T807) on postmortem brain tissue. *Ann Neurol.* 2015;78:787–800.
21. Lowe VJ, Curran G, Fang P, et al. An autoradiographic evaluation of AV-1451 tau PET in dementia. *Acta Neuropathol Commun.* 2016;4:58.
22. Shi Y, Murzin AG, Falcon B, et al. Correction to: Cryo-EM structures of tau filaments from Alzheimer's disease with PET ligand APN-1607. *Acta Neuropathol (Berl).* 2021;141:983.
23. Tagai K, Ono M, Kubota M, et al. High-contrast in vivo imaging of tau pathologies in Alzheimer's and non-Alzheimer's disease tauopathies. *Neuron.* 2021;109:42–58.e8.
24. Knight AC, Morrone CD, Varlow C, Yu WH, McQuade P, Vasdev N. Head-to-head comparison of tau-PET radioligands for imaging TDP-43 in post-mortem ALS brain. *Mol Imaging Biol.* 2023;25:513–527.
25. Varlow C, Vasdev N. Evaluation of tau radiotracers in chronic traumatic encephalopathy. *J Nucl Med.* 2023;64:460–465.
26. Schöll M, Lockhart SN, Schonhaut DR, et al. PET imaging of tau deposition in the aging human brain. *Neuron.* 2016;89:971–982.
27. Schwarz AJ, Yu P, Miller BB, et al. Regional profiles of the candidate tau PET ligand ^{18}F-AV-1451 recapitulate key features of Braak histopathological stages. *Brain.* 2016;139:1539–1550.
28. Marquié M, Siao Tick Chong M, Anton-Fernandez A, et al. [F-18]-AV-1451 binding correlates with postmortem neurofibrillary tangle Braak staging. *Acta Neuropathol (Berl).* 2017;134:619–628.
29. Wright JP, Goodman JR, Lin YG, et al. Monoamine oxidase binding not expected to significantly affect [^{18}F]flortaucipir PET interpretation. *Eur J Nucl Med Mol Imaging.* 2022;49:3797–3808.
30. Pascoal TA, Benedet AL, Tudorascu DL, et al. Longitudinal ^{18}F-MK-6240 tau tangles accumulation follows Braak stages. *Brain.* 2021;144:3517–3528.
31. Pascoal TA, Therriault J, Benedet AL, et al. ^{18}F-MK-6240 PET for early and late detection of neurofibrillary tangles. *Brain.* 2020;143:2818–2830.
32. Marquié M, Normandin MD, Meltzer AC, et al. Pathological correlations of [F-18]-AV-1451 imaging in non-Alzheimer tauopathies. *Ann Neurol.* 2017;81:117–128.
33. Stern RA, Adler CH, Chen K, et al. Tau positron-emission tomography in former National Football League players. *N Engl J Med.* 2019;380:1716–1725.
34. Marquié M, Aguero C, Amaral AC, et al. [^{18}F]-AV-1451 binding profile in chronic traumatic encephalopathy: a postmortem case series. *Acta Neuropathol Commun.* 2019;7:164.
35. Kroth H, Oden F, Molette J, et al. Discovery and preclinical characterization of [^{18}F]PI-2620, a next-generation tau PET tracer for the assessment of tau pathology in Alzheimer's disease and other tauopathies. *Eur J Nucl Med Mol Imaging.* 2019; 46:2178–2189.
36. Shoghi-Jadid K, Small GW, Agdeppa ED, et al. Localization of neurofibrillary tangles and beta-amyloid plaques in the brains of living patients with Alzheimer disease. *Am J Geriatr Psychiatry.* 2002;10:24–35.
37. Kepe V, Bordelon Y, Boxer A, et al. PET imaging of neuropathology in tauopathies: progressive supranuclear palsy. *J Alzheimers Dis.* 2013;36:145–153.
38. Omalu B, Small GW, Bailes J, et al. Postmortem autopsy-confirmation of antemortem [F-18]FDDNP-PET scans in a football player with chronic traumatic encephalopathy. *Neurosurgery.* 2018;82:237–246.
39. Schweighauser M, Arseni D, Bacioglu M, et al. Age-dependent formation of TMEM106B amyloid filaments in human brains. *Nature.* 2022;605:310–314.
40. Jiang YX, Cao Q, Sawaya MR, et al. Amyloid fibrils in FTLD-TDP are composed of TMEM106B and not TDP-43. *Nature.* 2022;605:304–309.
41. Chang A, Xiang X, Wang J, et al. Homotypic fibrillization of TMEM106B across diverse neurodegenerative diseases. *Cell.* 2022;185:1346–1355.e15.
42. Perneel J, Neumann M, Heeman B, et al. Accumulation of TMEM106B C-terminal fragments in neurodegenerative disease and aging. *Acta Neuropathol (Berl).* 2023;145:285–302.
43. Bigio EH, Wu JY, Deng HX, et al. Inclusions in frontotemporal lobar degeneration with TDP-43 proteinopathy (FTLD-TDP) and amyotrophic lateral sclerosis (ALS), but not FTLD with FUS proteinopathy (FTLD-FUS), have properties of amyloid. *Acta Neuropathol (Berl).* 2013;125:463–465.